


V. BRIEN¹,
A. DAUSCHER²
P. WEISBECKER¹
F. MACHIZAUD¹

Growth of a textured quasicrystalline phase in Ti-Ni-Zr films prepared by pulsed laser deposition

¹ Laboratoire de Science et Génie des Matériaux et de Métallurgie, UMR 7584, CNRS-INPL-UHP, Parc de Saurupt, ENSMN, 54042 Nancy Cedex, France

² Laboratoire de Physique des Matériaux, UMR 7556, CNRS-INPL-UHP, Parc de Saurupt, ENSMN, 54042 Nancy Cedex, France

Received: 7 June 2001 / Accepted: 18 February 2002
Published online: 3 June 2002 • © Springer-Verlag 2002

ABSTRACT The preparation in thin film form of the known icosahedral phase in Ti-Ni-Zr bulk alloys has been investigated as a function of substrate temperature. Films were deposited by pulsed laser deposition on sapphire substrates at temperatures ranging from room temperature to 350 °C. Morphological and structural modifications have been followed by grazing-incidence and θ -2 θ X-ray diffraction, transmission electron diffraction and imaging. Chemical composition has been analyzed by electron probe microanalysis. The in-depth variation of composition has been studied by secondary neutral mass spectroscopy. We show that pulsed laser deposition at 275 °C makes the formation of a 1- μ m-thick film of Ti-Ni-Zr quasicrystalline textured nanocrystallites possible.

PACS 68.55. Nq; 68.55. a; 68.55. Jk; 81.15. Fg

1 Introduction

Quasicrystals are known to exhibit a new range of combination of properties in comparison with their metallic compounds. Some icosahedral quasicrystalline Ti-based alloys, or related phases, have been shown by Kelton et al. and Nicula et al. [1, 2] to be able to reversibly store large amounts of hydrogen. As a matter of fact, the large number of tetrahedral sites in the structure, combined with the natural affinity of Ti and Zr atoms for hydrogen, makes the Ti-Ni-Zr quasicrystalline phase an excellent candidate for constitutive materials in batteries. The phase can actually absorb up to two hydrogen atoms for each metallic atom [3]. This performance makes this new phase a tangible alternative as a hydrogen storage material. In order to be able to use these materials for this goal, the feasibility of processing films must be proven as the optimization of the storage in such solid batteries needs the maximization of the surface/volume ratio of the material [4]. Pulsed laser deposition (PLD) was chosen as the preparation method because it has been shown to be a powerful method for preparing thin films of virtually any material, from pure elements to multi-component compounds [5]. The stoichiometry of the target is generally reproduced in the deposited film. In contrast to conventional deposition techniques, PLD

provides rather unusual growth conditions: very high supersaturation, bombardment by energetic particles and extremely high quenching rates for the condensing atoms. Consequently, the build-up of the film takes place far from equilibrium conditions, leading to the formation of metastable film structures. Significant differences in the structure and microstructure of simple metallic alloy films prepared by PLD have been found, as compared with films prepared by more conventional techniques [6, 7]. In fact, very few papers deal with the preparation of quasicrystals by laser ablation. Indeed, preparation of quasicrystalline films has most commonly been tackled using other techniques. For instance, post-annealing of sequential electron gun deposition of constitutive elements of the alloy has been used to prepare Al-Co films [8], Al-Cu-Fe films [9–11] and Al-Cu-Mg films [12]. Physical vapor deposition has also been used [13] to make Al-Cu-Fe films. Using laser ablation, Ichikawa et al. [14] have been the only team to obtain a pure quasicrystalline film in the Al-Pd-Mn system, while Teghil et al. [15] have obtained a mixture of the icosahedral φ phase and the crystalline β phase of the Al-Cu-Fe system. In this paper, we report for the first time on the preparation of quasicrystalline Ti-Ni-Zr thin films by PLD. Attention was focused on the optimization of the substrate deposition temperature. Particular care was taken to characterize the chemical composition and the changes in microstructure.

2 Experimental procedure

2.1 Synthesis

A pulsed Nd:YAG (Qantel, YG 571C) laser was used for the ablation process, working at the fundamental wavelength (1064 nm), a repetition rate of 10 Hz and pulse durations of 10 ns. The laser beam impinged at 30° with regard to the plane of the target, which was placed in a vertical position. The target was located at a distance of 45 mm from the substrate. The substrate was kept at the temperature T_s by the simple Joule effect of a small resistance located behind it (Fig. 1). The energy of the outgoing beam was monitored by an energy meter, allowing the estimation of the laser fluence used, 72 J/cm².

Experiments were conducted in a high vacuum chamber under an initial base pressure of 10^{-7} – 10^{-8} mbar, stabilizing at a value of one-decade order less after a few minutes of ablation.

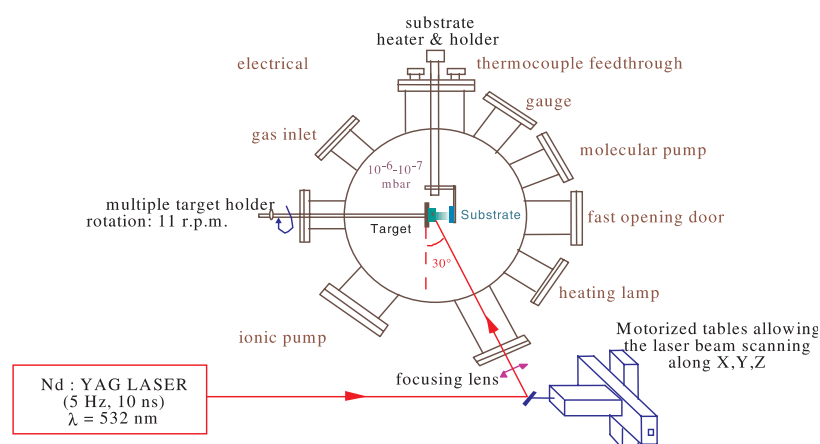


FIGURE 1 Schematic diagram of the pulsed laser deposition set-up

The targets used for the pulsed laser deposition were obtained from cutting Ti-Ni-Zr ingots, which were further polished with a SiC 1200 paper grid. The ingots were prepared by RF melting high-purity metals under a helium atmosphere in an induction furnace. Oxidation of Ti and Zr were prevented as far as it was possible by preparing them in an argon glove box. The targets presented as disks of 18 mm in diameter and 4 mm in thickness. The bulk materials were characterized by electron probe microanalysis (EPMA) on a CAMECA SX 50 and scanning electron microscopy (SEM) with a PHILIPS XL30G, in order to check the composition of the ingots and more particularly that the size of the different phases present in the bulk target were far smaller than the laser spot size used. The same target was used for the preparation of several consecutive films, provided a standard polishing was performed prior to each film deposition. This polishing ensured, amongst other things, the elimination of surface roughness of the target, which usually produces unwanted droplets on the film. Following the same goal, the combination of the non-linear motion of the laser beam through the computerized control of step-by-step motors [16] and the rotation of the target (11 r/min) was used to renew the irradiated area and to avoid crater formation.

Sapphire substrates oriented along their [0001] direction, used as received, were chosen as a substrate material due to their chemical inertness and role as diffusion barrier. The thick films obtained were all strongly adherent to their substrate and mirror-like. Typical deposition rates obtained were 1–8 Å/min.

The films were not further annealed as destructive oxidation systematically occurred during the process.

2.2 Characterization

The global composition of the films was characterized by EPMA, provided the films were thick enough (no substrate interference). Chemical depth profiles were obtained by secondary neutral mass spectroscopy (SNMS). All the chemical compositions are given within the experimental error of 1 at.%. The thicknesses were estimated by performing profilometry on the SNMS craters. Grazing-incidence X-ray diffraction (GXR) using Co $K_{\alpha 1}$ radiation and a curved detector (INEL CPS120) was performed at 0.5° incidence for the identification of the phases. GXR is an excellent technique

for obtaining information about the nature and the structure of the phases formed in thin films. It is, however, crucial to specify the geometric configurations of the atomic planes that diffract under such incidences. Indeed, as the curved detector collects X-rays spanning a 120° 2θ -range and the incidence angle is fixed at 0.5°, the atomic planes susceptible to being detected when in Bragg conditions are firstly those whose zone axis is perpendicular to the incident plane and parallel to the goniometer axis, and secondly those that make an angle of 0 to 60° with the surface. Such a diffraction geometry implies that a peak measured in the pattern at $2\theta_0$ indicates the presence of grains in the film, so orientated that the related family of planes are inclined at an angle of $\theta_0 = 0.5^\circ$ towards the surface. Carbon-coated copper electron microscopy grids were systematically installed just next to the substrate on the substrate holder inside the deposition chamber. Transmission electron microscopy (TEM) observations were carried out directly on the material deposited on these grids or by cutting a sample of film in the case of the thick 1- μm -film. A Philips CM200 with an accelerating voltage of 200 kV was used. The thickest film was also characterized by standard Bragg–Brentano classic θ – 2θ diffraction using Co $K_{\alpha 1}$ radiation and by 4-circles diffraction using the Co K_{α} radiation, in order to describe the observed texture. To do so, four pole figures were recorded. One recalls that a pole figure of type $[hkl]$ represents the angular distribution of intensities of the reflections of this $[hkl]$ Bragg family on a stereographic projection. Specifically, the sample was rotated through the angle φ about its normal direction and through the angle χ about the intersection of the reflecting plane and the sample plane. The origin of the angle χ was parallel to the normal direction of the film. The data were corrected and analyzed using TexevalTM software from Bruker Axs. Iso-intensity lines were chosen such that the most intense zones appeared on every pole figure. The error on measurement of χ (χ being then the radial angle on the pole figures) was checked on a monocrystalline Si sample and found to be around 1°.

3 Results and discussion

3.1 Chemical congruence

The study of the chemical transfer between the targets used and the films obtained revealed that, unfortunately,

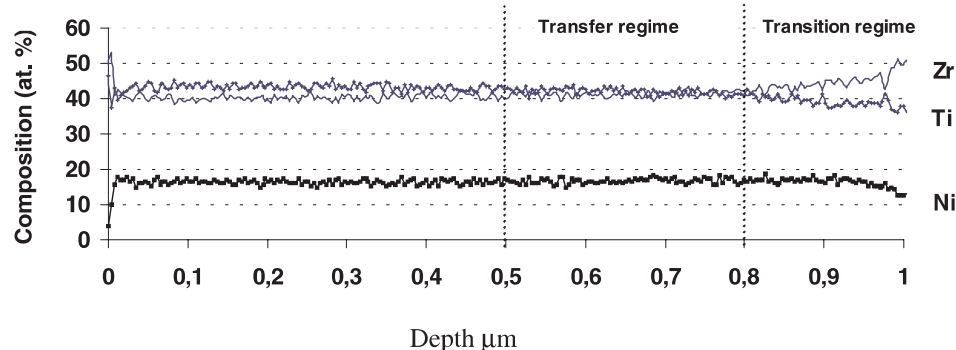


FIGURE 2 In-depth ternary chemical profile obtained by SNMS on a 1 μm Ti-Ni-Zr film deposited at room temperature from a $\text{Ti}_{45}\text{Ni}_{17}\text{Zr}_{38}$ ingot, imaging the chemical transfer chronology. Substrate is on the right, above 1 μm

the ternary Ti-Ni-Zr system does not transfer the chemistry as faithfully as expected. Two points have been made clear.

To obtain the desired $\text{Ti}_{41.5}\text{Ni}_{17}\text{Zr}_{41.5}$ composition, which was identified by electron dispersion spectroscopy by Kelton et al. [17] to be the nominal icosahedral phase composition, a target of $\text{Ti}_{45}\text{Ni}_{17}\text{Zr}_{38}$ composition was found to give the best results at room temperature. Indeed, a 1- μm -thick film of Ti-Ni-Zr was obtained keeping the substrate temperature at 25 °C. Its atomic composition was measured by EPMA and found to be $\text{Ti}_{42}\text{Ni}_{18}\text{Zr}_{40}$, and fairly homogeneous across the whole deposited surface.

Since the composition measured by EPMA represents the integration of around 1 μm^3 volume, depth chemical profiling has been investigated by SNMS in the same 1 μm film and is shown in Fig. 2. From this profile it is possible to follow the chemical transfer chronology. Close to the interface with the substrate, the stoichiometry transfer from target to substrate is far from being achieved: larger amounts of Zr, to the detriment of Ni and Ti, are observed. The wanted stoichiometry, $\text{Ti}_{41.5}\text{Ni}_{17}\text{Zr}_{41.5}$ (different from the target), can only be observed in the 0.8–0.5 μm range of Fig. 2, after a transition regime that lasts roughly 30 min. This duration is much larger than that necessary to erode the whole target surface at one time, meaning that the Zr enrichment in the film is certainly not only linked to Zr target surface segregation but also to preferential erosion. The corresponding depletion in Ti may arise from re-sputtering from the film surface. Thus, the wanted stoichiometry is only reached after having deposited around 0.2 μm and presents the most interesting transfer regime at 0.3 μm (0.8 to 0.5 μm in Fig. 2). Provided a pre-ablation of 30 min is assured prior to any film growth, the first 0.3 μm of deposited material will have the right composition within 1 at. % and the following layers within 2 at. %, presenting the slight chemical gradient as shown in Fig. 2 (range 0–0.5 μm).

3.2 Dependence of the nature and structure of the films versus the substrate temperature

In order to be able to practice electron microscopy, the films deposited were designed to be about 50 nm in thickness. The structures of the films were all analyzed by GXRD and TEM.

3.2.1 X-ray diffraction results. The X-ray diffraction pattern of the film deposited at room temperature, presented in Fig. 3, shows a broad maximum, which characterizes an amorphous

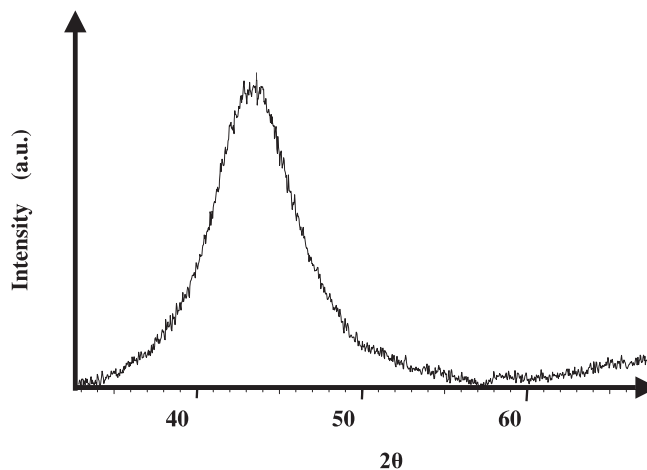


FIGURE 3 Grazing-incidence (0.5°) X-ray diffraction pattern of the Ti-Ni-Zr film deposited at room temperature ($\lambda = 0.178897$ nm). Background has been removed

structure. In order to be free from this unwanted amorphous phase, more energy was brought to the substrate in order to crystallize the deposit. A series of film depositions were prepared, heating the sapphire substrate during the laser ablation process. Chosen temperatures were 160 °C, 240 °C, 295 °C and 350 °C, and results of GXRD are respectively shown in Fig. 4. When identified, the indexation of the peaks has been placed on the figures. The system of indexation by Cahn et al. [18] was used for the quasicrystalline phase. The reader will find in the Appendix a correspondence table for the most intense peaks with the Bancel et al. [19] system of indexation. Details on the approximant W phase found to appear at lower temperatures can be found in [20].

Figure 4 presents the GXRD pattern of the film prepared at 295 °C. It exhibits reflections that could be identified as the three main peaks of the Ti-Ni-Zr icosahedral structure: the $(2/3\ 0/0\ 1/2)$, the $(2/4\ 0/0\ 0/0)$ and the $(4/6\ 0/0\ 0/0)$ reflections. Their corresponding experimental Q_{\parallel} are listed in Table 1. One recalls $Q_{\parallel} = (2\pi/a_{6D})(N + M\tau)/(2(2 + \tau))^{1/2} = (2\pi/a_{6D})f(N, M)$, with the golden mean and $Q_{\parallel} = 4\pi \sin \theta/\lambda$, setting $f(N, M) = (N + M\tau)/(2(2 + \tau))^{1/2}$, leading to:

$$a_{6D} = (2\pi/Q_{\parallel})f(N, M) \quad (1)$$

The six-dimensional parameter value was found to be $a_{6D} = 0.741 \pm 0.001$ nm (quasi-lattice $a_q = 0.520 \pm 0.001$ nm).

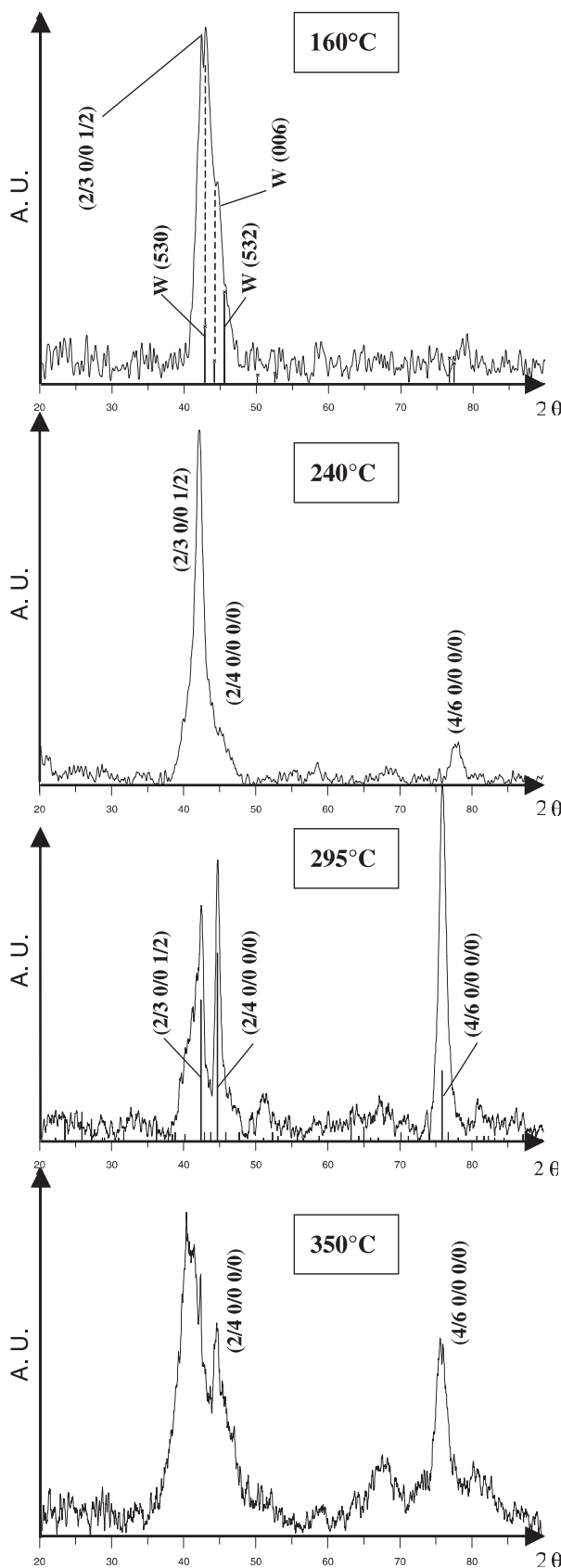


FIGURE 4 Set of grazing-incidence X-ray diffraction patterns of the Ti-Ni-Zr films deposited at various temperatures, 160–350 °C. The vertical lines indicate the position of the main peaks of the quasicrystalline phase and the W phase. See deconvolution of the $2\theta = 42^\circ$ peak of the 240 °C X-ray pattern in Fig. 5 and Table 1

The increase in the lattice parameter of 0.6%, when compared with the values obtained by high-resolution X-ray diffraction (synchrotron) found in the literature ([2], $a_{6D} = 0.7368 \pm 4 \times 10^{-4}$ nm, $a_q = 0.5210 \pm 4 \times 10^{-4}$ nm), can probably be explained by the oxygen absorption of the lattice (SNMS dosage of oxygen actually gives 1.5 at. %) or by the phenomenon of lattice expansion usually observed for intermetallic compound films deposited by the PLD technique because of very intense condensation speeds [21]. The comparison of the relative intensities of the icosahedral peaks with those usually obtained in the literature [2, 3, 22–26] for the bulk phase informs us that the icosahedral grains are not 100% randomly distributed. The relative intensities of all the peaks show that the icosahedral phase is the main phase present in that film. The shoulders of the 42° peak and the 51° peak indicate that the film also contains an unwanted second phase, which becomes predominant at higher temperature (350 °C).

At lower substrate temperature, i.e. 240 °C, deconvolution was necessary to understand the signal obtained from GXRD around $2\theta = 42^\circ$ (Fig. 4). As Fig. 5 illustrates, the signal could be decomposed into 3 peaks. The details of all the peaks in this pattern, namely position, full width at half maximum (FWHM), indexation, deduced parameter and size of the diffracting particles, calculated using Scherrer law, are given in Table 2. The most intense peak in the pattern does not correspond to any phase within the ICDD database (Powder Diffraction file™ Release 2000) or to any peak of a phase usually met in work dealing with the preparation of the Ti-Ni-Zr icosahedral phase. The only possible match is the $(2/3\ 0/0\ 1/2)$ reflection of the icosahedral structure. The six-dimensional parameter then obtained is $a_{6D} = 0.745 \pm 0.002$ nm ($a_q = 0.527 \pm 0.002$ nm). The missing peaks of the other icosahedral structure linked to this one suggest that the grains of this domain (labeled 1) are strongly textured (to be dealt with further). The average size of the crystallites of this domain was 16 nm. The analysis of the other peaks evidences that the film also contained a second domain (labeled 2), made of smaller imperfect quasi-crystalline crystallites (see Table 1). Their average size was around 4 nm.

At 160 °C, the film seems to be formed by a mixture of the icosahedral phase and another phase, producing a spreading of the large complex peak centered around $2\theta = 42^\circ$. This enlargement could be due to residual presence of the amorphous phase observed at room temperature or to the presence of another phase. One probable phase is the known 1/1 approximant: the W phase [20]. Indeed, the (530), (532) and (006) peaks of the W phase placed on the pattern correspond rather well to the presence of the different shoulders on the peak. It is, however, rather difficult to conclude. Indeed, the W phase usually appears at higher temperatures than the icosahedral during annealing treatment of the bulk material [27].

The patterns attesting the presence of the icosahedral phase display different sets of structure peaks, depending upon the temperature substrate. The grains are therefore orientated differently against the substrate at different temperatures and this suggests that the different textures of this phase might be obtained by changing the temperature.

$Q_{ }$ nm ⁻¹ from GXRD	a_{6D} nm from GXRD	$Q_{ }$ nm ⁻¹ from TEMDP	a_{6D} nm from TEMDP	$Q_{ }$ nm ⁻¹ from 4-circles cumulated pattern	a_{6D} nm from 4-circles cumulated pattern	N/M	Indices
(295 °C)	(295 °C)	(240 °C and 295 °C)	(240 °C and 295 °C)	(275 °C)	(275 °C)	Cahn et al. [18]	
	±0.002 nm		±0.04 nm		±0.001 nm		
—	—	15.0	0.71	—	—	6/9	1/2 0/1 0/0
—	—	16.7	0.73	—	—	8/12	2/2 0/0 0/0
—	—	24.0	0.74	—	—	18/25	1/4 0/1 0/0
25.45	0.741	25.7	0.73	25.24	0.746	18/29	2/3 0/0 1/2
26.74	0.740	27.2	0.73	26.57	0.745	20/32	2/4 0/0 0/0
—	—	30.8	0.73	30.09	0.746	26/41	3/4 0/1 0/0
—	—	39.2	0.72	—	—	42/65	4/5 0/0 1/0
43.24	0.741	43.9	0.73	43.09	0.743	52/84	4/6 0/0 0/0
—	—	—	—	49.96	0.743	70/113	4/7 0/0 1/2
—	—	—	—	50.60	0.744	72/116	4/6 0/0 2/4

TABLE 1 Lists of the $Q_{||}$ values obtained from the experimental measurements on X-ray or transmission electron diffraction patterns, with their indexation and allowing the calculation of the six-dimensional lattice parameter a_{6D} of the icosahedral phase ((1), see the text)

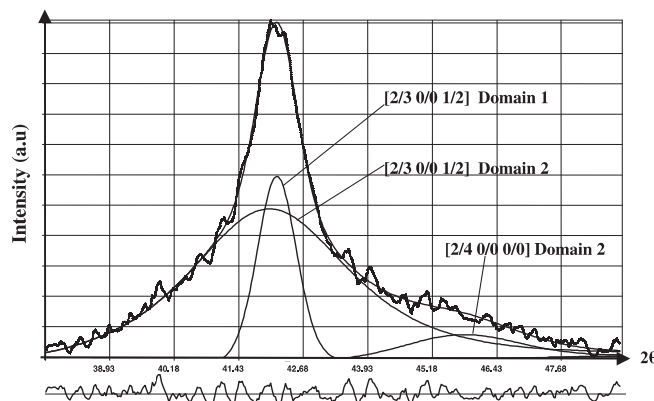


FIGURE 5 Detail of deconvolution using Winfit software* of the 42° peak of the GXRD pattern obtained from the film prepared at 240 °C. The lower curve is the difference between the experimental data and the fit. See Table 1 for numerical details of the deconvoluted peaks. (* Winfit 1.2, S. Krumm, Institut für Geologie, Erlangen)

3.2.2 TEM results. TEM diffraction and TEM imaging in the dark field were also performed in order to assess the size and geometry of the grains. Figure 6 shows a pattern obtained for the sample prepared at 240 °C, and Fig. 7 for the one deposited at 295 °C. Whatever the temperature of the sample, the diffraction patterns exhibit well-defined rings, indicating that all the films are made of small grains, and present strong radial but symmetric heterogeneities so that the ring intensity contrasts make symmetric arcs. Such arcs are typical of the presence of textures and are present in all diffraction patterns. In the same way, the rings of the icosahedral structure are systemati-

cally present, but the distribution of intensity on the rings is different from one pattern to another and depends on the temperature T_s .

Since the X-ray diffraction results of the films prepared at 240 °C and 295 °C show these temperatures are the most appropriate for maximizing the volume of the icosahedral phase, only TEM data from samples obtained at these temperatures are presented (Fig. 6a and b). Again, Cahn et al. [18] indexation was used and placed on the figures.

Table 1 lists the values of $Q_{||}$ obtained from the measurements of the diameter of the rings on either pattern (240 °C or 295 °C) since they exhibit the same inter-reticular distances. The parameters found were: $a_{6D} = 0.72 \pm 0.04$ nm ($a_q = 0.52 \pm 0.04$ nm). The difference of 3% with what was obtained using GXRD (see Sect. 3.2.1) for the films is of the same order as the 5% error coming from the TEM technique itself, despite calibration.

As shown in Fig. 6a, on top of the rings belonging to the icosahedral structure, a diffuse intensity can be noticed on the TEM pattern made using the 240 °C sample around rings (1/4 0/1 0/0), (2/3 0/0 1/2) and (2/4 0/0 0/0), corresponding to the identified crystallites of domain 2 (see analysis of GXRD data). At 295 °C, the icosahedral domain 2 has disappeared.

The systematic dark-field patterns, performed by localizing an aperture on an arc of the fifth diffused paraxial ring (2/4 0/0 0/0) of the different samples, allows an estimation of the sizes of the crystallites. These are listed in Table 3 against the substrate temperature T_s ; smaller and larger values are indicated. Size distribution seems to be simple and the average size of the particles is apparently in the middle of the ranges. Size homogeneity was, however, checked by system-

TABLE 2 Numerical data of peaks on the GXRD pattern of the film prepared at 240 °C. The data of the 77.89° peak are directly measured on the pattern; the other information was obtained by deconvolution of the 42° peak. See Figs. 4 and 5 for the pattern and the deconvolution curves

$2\theta(^{\circ})$	42.010	42.168	45.751	77.890
FWHM ($^{\circ}$)	3.493	0.693	2.464	2.8
Indexation	2/3 0/0 1/2	2/3 0/0 1/2	2/4 0/0 0/0	4/6 0/0 0/0
a_{6D} (nm)	0.748	0.745	0.725	0.725
Estimation of the size of particles (nm)	≈ 3	≈ 16	≈ 4	≈ 5
Domain	2	1	2	2

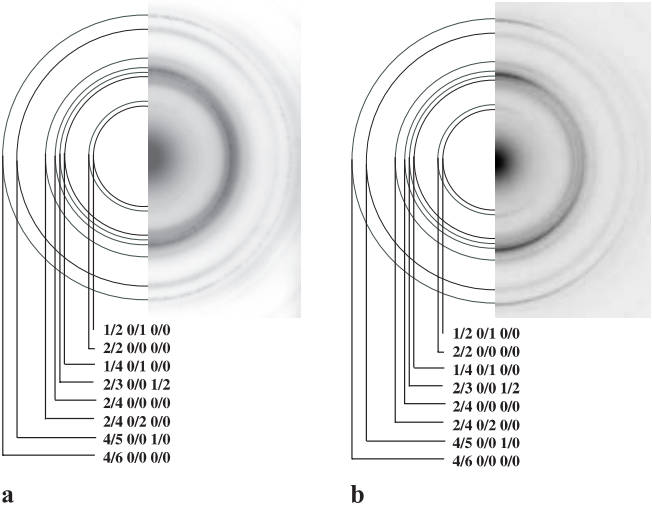


FIGURE 6 TEM diffraction pattern of films deposited at: **a** 240 °C and **b** 295 °C

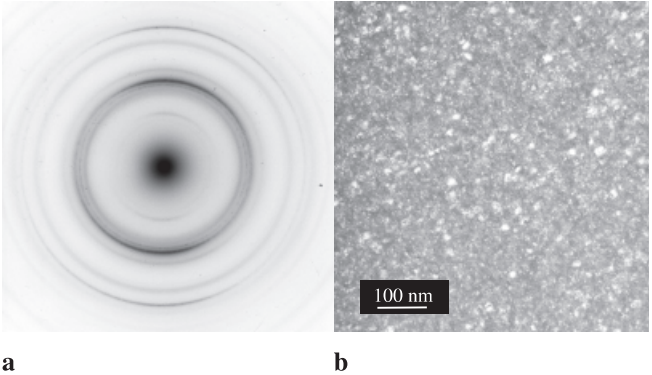


FIGURE 7 Electron diffraction pattern (**a**) confirming the presence of a texture in the 295 °C film and dark-field image (**b**) made for the measurement of the average size of the grains in the same film

T_s (°C)	160	240	295	350
Size (nm) (mimum–maximum)	4–8	2–10	2–19	2–10

TABLE 3 Average size of the grains of Ti-Ni-Zr 50-nm-thick films versus the substrate temperature T_s

atic measurements on several images. The sizes reached up to 10 or even 20 nm for $T_s = 295$ °C.

3.3 Growth of a thick icosahedral-textured Ti-Ni-Zr film sample

As presented above, a substrate temperature of 240 °C leads to the formation of the icosahedral phase, divided up in two domains. One of the domains is made of textured crystallites and the other is made of smaller non-textured grains. However, working at 295 °C has been shown to lead to a mixture of the icosahedral phase and a high-temperature crystalline phase. Consequently, 275 °C was the temperature chosen for the preparation of a monophase quasicrystalline film, hoping for a possible texture. To get a complete description of the expected texture of the film, its target thickness was around 1 μm . Two hours of ablation were necessary to obtain the right thickness.

The chemical composition of the film obtained by EPMA gave $\text{Ti}_{42.9}\text{Ni}_{15.6}\text{Zr}_{41.5}$, to be compared to $\text{Ti}_{41.5}\text{Ni}_{17}\text{Zr}_{41.5}$, the composition found for the quasicrystalline phase in bulk by other authors [17].

The Bragg–Brentano, GXRd and 4-circles diffraction patterns performed on the thick film, respectively presented in Fig. 8a, b and c, bring complementary, consistent structural information. The Bragg–Brentano diffraction pattern exhibits peaks that could be indexed as being (2/3 0/0 1/2) and (4/6 0/0 1/4) of the icosahedral structure. The GXRd pattern of the same film exhibits other peaks of the icosahedral structure, like (2/4 0/0 0/0) and (4/6 0/0 0/0), which are the most intense. The presence of these different reflections on the two patterns attests the presence of a texture in the film. To precisely determine this texture, 22 scans were

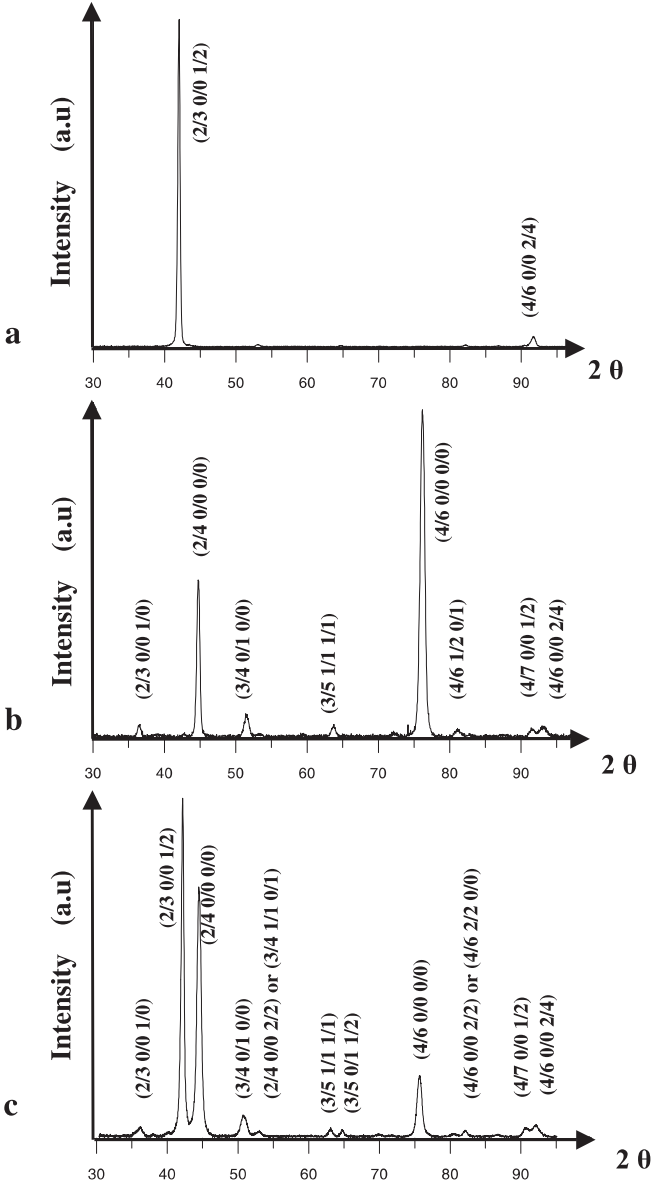


FIGURE 8 X-ray diffraction patterns performed on a Ti-Ni-Zr film deposited by PLD at 275 °C: **a** Bragg–Brentano θ – 2θ diffraction pattern; **b** grazing-incidence (0.5°) diffraction pattern; **c** addition of the 22 scans recorded at different χ ($\chi = 0$ to 55°) performed on a four-circles diffractometer ($\lambda = 0.178897$ nm)

recorded at different χ on the 4-circles diffractometer and added in order to cumulate and visualize all the possible Bragg reflections of the film on the same pattern. The acquisition of the 22 cumulated scans was done with χ ranging from 0 to 55°, assuring a φ rotation of the sample at 600 rpm (Fig. 8c). Such an acquisition allows us to visualize all the possible Bragg diffractions of all the crystallographic planes present in the film for Bragg angles located between $2\theta = 30^\circ$ and $2\theta = 96^\circ$. The pattern obtained exhibits a set of reflections, which can be attributed to a primitive (*P*-type) hypercubic lattice of an icosahedral phase (icosahedral group $m\bar{3}\bar{5}$). Indexation of all peaks has been inserted in the pattern. The lattice parameter refinement has been performed and gives $a_{6D} = 0.744 \pm 0.001$ nm ($a_q = 0.526 \pm 0.001$ nm).

The texture was specified by recording pole figures for different planes (Fig. 9): chosen Bragg peaks are firstly $2\theta = 42^\circ$ and 92.3° , and secondly 44° and 76° , corresponding to the main reflections of Fig. 8a and b.

According to the indexation performed above, the 42° and 92.3° peaks come from the same family of planes perpendicular to the five-fold axes; indeed, the 92.3° peak corresponds to a second-order reflection. Figure 9a exhibits a maximum of diffraction around $\chi = 0^\circ$ in the shape of a half-circle located at $\chi = 6.4^\circ$. This family gives very intense maxima at $\chi = 56^\circ$ and $\chi = 68.5^\circ$. Measurements on the pole figure (Fig. 9a and b) of the angle $\Delta\chi$ between the most intense domains lead to the following values: $62.1 \pm 2^\circ$ and $62.4 \pm 2^\circ$ ($68.5^\circ - 6.4^\circ$ or $56^\circ + 6.4^\circ$). This is to be compared with 63.4° , which is the angle between two five-fold axes in the icosahedral structure [28, 29]. Comparison of Fig. 9a and b shows they present exactly the same aspect, with an attenuation in intensity from Fig. 9a to b. The small half-circle is also positioned exactly at $\chi = 6.4^\circ$, and despite the weak traces of diffraction intensity, could be recorded at the position corresponding to the maxima of the half-circle located at 56°

and 62.4° . This unambiguously confirms these two peaks are related to the same family of planes. A compression of the parameter of around 1% is also noticed when calculating it from the position of the $(2/3\ 0/0\ 1/2)$ reflection when scanning at $\chi = 6^\circ$ and $\chi = 56^\circ$: one finds 0.748 nm at 6° and 0.738 nm at 56° .

A similar analysis was performed on the two most intense peaks appearing in Fig. 8b (GXR). Figure 9c and d presents the pole figures of the 44° and 76° peaks. The identical distribution of intensity on the two pole figures confirms they represent parallel planes. Indeed, the indexation informs us that the two peaks are Bragg peaks of families of planes perpendicular to the two-fold axes, and so are linked by a τ deflation. Similarly, $88.5 \pm 2^\circ$ and $89.5 \pm 2^\circ$ ($24.5^\circ + 64^\circ$ or $37.5^\circ + 52^\circ$) were the angles measured between, respectively, the rings labeled 1 and 4 of Fig. 9c, and the rings labeled 2 and 3. These values are to be compared with 90° , the angle between two-fold axes in the icosahedral structure.

In addition to all this analysis, it was possible to check that the angles between what are deduced to be reflections linked to planes perpendicular to the five-fold and two-fold axes really are fully compatible with the icosahedral structure: indeed $31.5 \pm 2^\circ$ ($56^\circ - 24.5^\circ$) and $31.0 \pm 2^\circ$ ($68.5^\circ - 37.5^\circ$) were measured. This is to be compared with the angle between five-fold and two-fold axes: 31.7° . In the same way, it has been carefully checked that the family of planes $(2/4\ 0/2\ 0/0)$ perpendicular to the three-fold axes give compatible angles (not presented here). Such a texture study shows that the planes perpendicular to the five-fold axes of the icosahedral Ti-Ni-Zr phase grow nearly parallel to the surface film (inclination of 6.4°). The texture observed here could be described as a non-homogeneous fiber tilted at 6.4° with respect to the normal of the film. Standard fiber textures are very often met in the growth of thin films [30–32]. The angle of the maximum of the texture with respect to the normal of the film, and probably also the non-homogeneous distribution of intensities, could have been produced by the inclination of the symmetric center of the plasma plume inside the laser chamber with regard to the normal of the substrate [33].

In the light of this four-circles diffraction investigation, it is rather trivial to understand why only reflections from planes perpendicular to five-fold axes are visible in Fig. 8a (Bragg–Brentano diffraction) and that only the ones perpendicular to two-fold axes are visible in Fig. 8b (GXR). Indeed, the geometrical configurations of the GXR and Bragg–Brentano diffraction techniques determine that in Bragg–Brentano diffraction, only those Bragg planes parallel to the film surface diffract towards the detector, and that in GXR, only the planes making an angle with the film surface in the range 0 to 60° and equal to their Bragg angle diffract towards the curved detector. Thus, as Fig. 9 shows, the $[2/3\ 0/0\ 1/2]$ and the $[4/6\ 0/0\ 2/4]$ reflections diffract near $\chi = 0^\circ$, explaining why they will be detected on a Bragg–Brentano pattern. In the same way, the $[2/4\ 0/0\ 0/0]$ reflection is present in the GXR pattern because the film contains related planes located around its Bragg angle, 22° , as the ring labeled 1, and localized around 24.5° , as confirmed in Fig. 9c. $[4/6\ 0/0\ 0/0]$ is

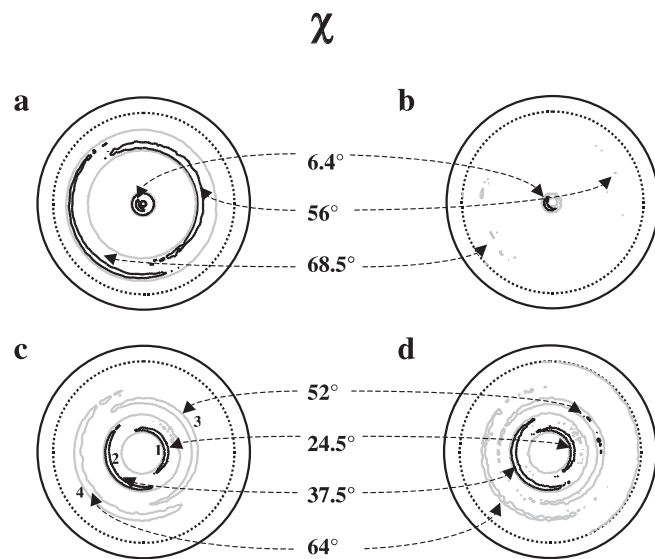


FIGURE 9 Pole figures recorded on a Ti-Ni-Zr film deposited by PLD at 275°C on a four-circles diffractometer of the $(2/3\ 0/0\ 1/2)$ peak at $2\theta = 42^\circ$ (a); $(4/6\ 0/0\ 2/4)$ peak at $2\theta = 92.3^\circ$ (b); $(2/4\ 0/0\ 0/0)$ peak at $2\theta = 44^\circ$ (c); and $(4/6\ 0/0\ 0/0)$ peak at $2\theta = 76^\circ$ (d). The dotted circle is the limit of measurements

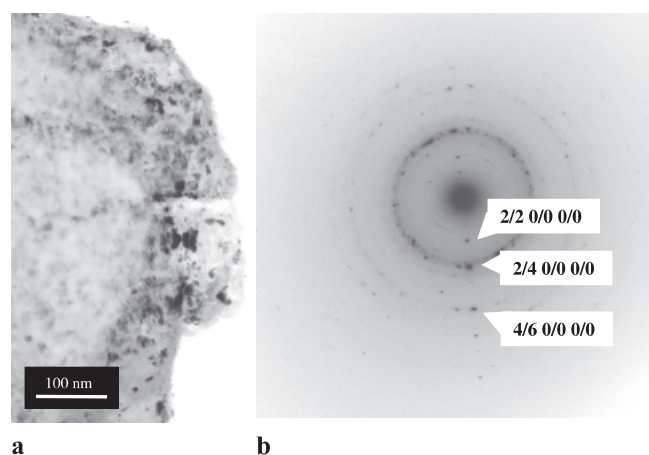


FIGURE 10 Film prepared at 275 °C: **a** bright-field image showing the typical size of the grains; and **b** selected-area diffraction pattern of a bigger grain than the average ones observed in the 1- μ m-film prepared at 275 °C

also detected in the GXRD pattern because the corresponding diffraction planes are found on Fig. 9d around $\chi = 37.5^\circ$ (Bragg angle = 38°).

To complete this study, TEM has been performed (Fig. 10). Most parts of the film produced a diffraction pattern made of dotted rings. Imaging informed us that the nanocrystallites are slightly bigger than in the films prepared at other temperatures (13 ± 4 nm, Fig. 10a). Some rare larger grains have also been noticed, producing a line of sharp Bragg spots, well aligned in a sequence of distances to the center of the pattern in τ ratios (Fig. 10b). Unfortunately, the thickness and configuration of those grains did not allow us to obtain a pattern along a zone axis of the structure. This diffraction line can be a systematic line from the five-fold electron diffraction pattern of an icosahedral structure or a systematic line from a pseudo-five-fold diffraction pattern of an approximant to the Ti-Ni-Zr quasicrystal [23].

4 Conclusions

This is the first report on the preparation of a film of the quasicrystalline Ti-Ni-Zr phase. Successful preparation was obtained using the PLD technique. Experimental conditions of preparation were found and were such that the films do not need any further thermal treatment. The one-micron film synthesized presented the $\text{Ti}_{41.5}\text{Ni}_{17}\text{Zr}_{41.5}$ icosahedral phase composition, the composition of which is known in bulk material to within about 2 at. %. It was made of icosahedral nanosized grains, presenting a texture along a five-fold axis slightly tilted ($\approx 6^\circ$) from the normal to the film. The atomic planes have also been shown to be stressed in the directions perpendicular to the growth, as usually observed in such elaborate films. However, rare approximant or icosahedral grains have been noticed in the film, much bigger than the nanosized grains. The films grown were all strongly adherent to their substrate, thanks to the small-sized grains. Investigations performed also suggest that different kinds of textures might be obtained by changing the substrate temperature during deposition. Confirmation of this would be extremely interesting, as hydrogen storage

is the most promising industrial application of the phase. One could then study whether energy storage depends on film texture.

ACKNOWLEDGEMENTS The authors would like to thank J.M. Dubois for having suggested this study. They also would like to thank J.P. Haeussler and J.B. Ledeuil for their assistance in microprobe measurements, and S. Weber for SNMS experiments. We are most grateful to F. Brillancourt from the LCTMR laboratory (CNRS France) for her help in preparing the ingots and to A. Percheron (LCTMR) for her constant interest in this work.

Appendix

Cahn et al. [18] Indexation system	Cahn et al. [18] N/M	Bancel et al. [19] Indexation system	Order of symmetry of the axis of the same indices
2/3 0/0 1/2	18/29	1/0 0/0 0/0	5
2/4 0/0 0/0	20/32	1/1 0/0 0/0	2
3/4 0/1 0/0	26/41	1/1 1/1 0/1	3
4/6 0/0 0/0	52/84	1/0 1/0 0/0	2
4/6 0/0 2/4	72/116	2/0 0/0 0/0	5

Correspondence between two systems of indexation of the icosahedral structure for the most intense reflections. The symmetry of the axes perpendicular to the indexed planes is given in the right-hand column.

REFERENCES

- 1 K.F. Kelton, P.C. Gibbons: *Mat. Res. Soc. Bull.* **22**, 69 (1997)
- 2 R. Nicula, A. Jianu, A.R. Birirs, D. Lupu, R. Manaila, A. Devenyi, C. Kumpf, E. Kurpel: *Eur. Phys. J. B* **3**, 1 (1998)
- 3 A.M. Viano, E.H. Majzoub, R.M. Stroud, M.J. Kramer, S.T. Misture, P.C. Gibbons, K.F. Kelton: *Phil. Mag. A* **78**, 131 (1998)
- 4 J.M. Tarascon, A. Percheron: *L'Actualité Chimique, Lettres des Départements Scientifiques du CNRS*, Vol. 3 No. 65. (Société Française de Chimie, EDP Science SA, Les Ulis, France 1998)
- 5 D.B. Chrisey, G.K. Hubler: *Pulsed Laser Deposition of Thin Films* (Wiley, New York 1994)
- 6 M. Störmer, H.U. Krebs: *J. Appl. Phys.* **78**, 7080 (1995)
- 7 H.U. Krebs: *Int. J. Non-Equil. Proc.* **10**, 1 (1997)
- 8 E. Emeric, P. Gas, G. Clugnet, C. Bergman: *Mat. Sci. Eng.* **50**, 285 (2000)
- 9 F. Giroud: *Ph.D. Thesis* (Université J. Fourier, Grenoble 1998)
- 10 C. Bergman, E. Emeric, P. Donnadieu, J.M. Dubois, P. Gas: *Proc. Fifth Int. Conf. on Quasicrystals*, Avignon, France, 22–26 May 1995, ed. by C. Janot, R. Mosseri (World Scientific, Singapore 1995)
- 11 E. Emeric, C. Bergman, J.M. Dubois, G. Clugnet, P. Gas: *Proc. of the Sixth Int. Conf. on Quasicrystals*, Tokyo, Japan, 26–30 May 1997, ed. by S. Takeuchi, T. Fujiwara (World Scientific, Singapore 1998)
- 12 C. Roth, R. Haberkern, P. Haeussler: *Colloquium Quasicristaux, GDR CINQ* (Paris, France, 5–7 June 1996) unpublished
- 13 J.L. Joulaud: *Ph.D. Thesis* (Université Paris VI, 1997)
- 14 N. Ichikawa, O. Matsumoto, T. Hara, T. Kitahara, T. Yamauchi, T. Matsuda, T. Takeuchi, U. Mizutani: *Jpn. J. Appl. Phys.* **33**, 736 (1994)
- 15 R. Teghil, L. D'Alessio, M.A. Simone, M. Zaccagnino, D. Ferro, D.J. Sordelet: *Appl. Surf. Sci.* **168**, 267 (2000)
- 16 A. Jacquot, M.O. Boffoué, B. Lenoir, A. Dauscher: *Appl. Surf. Sci.* **156**, 169 (2000)
- 17 K.F. Kelton, W.J. Kim, R. Stroud: *Appl. Phys. Lett.* **70**, 3230 (1997)
- 18 J.W. Cahn, D. Shechman, D. Gratias: *J. Mater. Res.* **1**, 13 (1986)
- 19 P.A. Bancel, P.A. Heiney, P.W. Stephens, A.I. Goldman, P.M. Horn: *Phys. Rev. Lett.* **54**, 2422 (1985)
- 20 W.J. Kim, P.C. Gibbons, K.F. Kelton: *Phil. Mag.* **76**, 199 (1997)

- 21 H.U. Krebs, O. Bremert, M. Störmer, T. Luo: Appl. Surf. Sci. **86**, 90 (1995)
- 22 S.A. Sibirtsev, V.N. Chebotnikov, V.V. Molokanov, Y.K. Kovneristy: JETP Lett. **47**, 744 (1988)
- 23 V.V. Molokanov, V.N. Chebotnikov: J. Non Crystal. Solids **789**, 117 (1990)
- 24 X. Zhang, R.M. Stroud, J.L. Libbert, K.F. Kelton: Phil. Mag. B **70**, 927 (1994)
- 25 A.M. Viano, R.M. Stroud, P.C. Gibbons, A.F. McDowell, M.S. Conradi, K.F. Kelton: Phys. Rev. B **51**, 12026 (1995)
- 26 A.M. Viano, A.F. McDowell, M.S. Conradi, R.M. Stroud, P.C. Gibbons, K.F. Kelton: *Quasi-Crystals*, ed. by C. Janot, R. Mosseri (World Scientific Publishing, Singapore 1995)
- 27 W.J. Kim, K.F. Kelton: Phil. Mag. A **72**, 1397 (1995)
- 28 C. Janot: *Quasi-Crystals, A Primer*, 2nd edn. (Oxford Science Publications, Oxford 1994)
- 29 D. Shechtman, I. Blech, D. Gratias, J.W. Cahn: Phys. Rev. Lett. **53**, 20 (1984)
- 30 D.B. Knorr, J.A. Szpunar: J. Mater. **46**, 42 (1994)
- 31 P. Coulomb: *Les Textures dans les Métaux de Réseau Cubique* (Dunod, Paris 1972)
- 32 H. Bunge: *General Outline and Series Expansion Method in Quantitative Texture Analysis*, ed. by H.J. Bunge, C. Esling (D.G.M. Inform, Frankfurt, Germany 1986)
- 33 U. Shultz, H. Oettel, W. Bunk: Z. Metallkd. **87**, 488 (1996)